the FEBS Journal

The binding of IMP to Ribonuclease A

George N. Hatzopoulos[1], Demetres D. Leonidas[1], Rozina Kardakaris[1], Joze Kobe[2] and Nikos G. Oikonomakos[1,3]

1 Institute of Organic & Pharmaceutical Chemistry, The National Hellenic Research Foundation, Athens, Greece
2 National Institute of Chemistry, Laboratory for Organic Synthesis and Medicinal Chemistry, Ljubljana, Slovenia
3 Institute of Biological Research & Biotechnology, The National Hellenic Research Foundation, Athens, Greece

Keywords
ribonuclease A, X-ray crystallography, IMP, structure assisted inhibitor design

Correspondence
D. D. Leonidas, Institute of Organic and Pharmaceutical Chemistry, The National Hellenic Research Foundation, 48 Vas. Constantinou Avenue, 11635 Athens, Greece
Fax: +30 210 7273831
Tel: +30 210 7273841
E-mail: ddl@eie.gr

(Received 1 April 2005, revised 13 June 2005, accepted 15 June 2005)

doi:10.1111/j.1742-4658.2005.04822.x

The binding of inosine 5′ phosphate (IMP) to ribonuclease A has been studied by kinetic and X-ray crystallographic experiments at high (1.5 Å) resolution. IMP is a competitive inhibitor of the enzyme with respect to C>p and binds to the catalytic cleft by anchoring three IMP molecules in a novel binding mode. The three IMP molecules are connected to each other by hydrogen bond and van der Waals interactions and collectively occupy the $B_1R_1P_1B_2P_0P_{-1}$ region of the ribonucleolytic active site. One of the IMP molecules binds with its nucleobase in the outskirts of the B_2 subsite and interacts with Glu111 while its phosphoryl group binds in P_1. Another IMP molecule binds by following the retro-binding mode previously observed only for guanosines with its nucleobase at B_1 and the phosphoryl group in P_{-1}. The third IMP molecule binds in a novel mode towards the C-terminus. The RNase A–IMP complex provides structural evidence for the functional components of subsite P_{-1} while it further supports the role inferred by other studies to Asn71 as the primary structural determinant for the adenine specificity of the B_2 subsite. Comparative structural analysis of the IMP and AMP complexes highlights key aspects of the specificity of the base binding subsites of RNase A and provides a structural explanation for their potencies. The binding of IMP suggests ways to develop more potent inhibitors of the pancreatic RNase superfamily using this nucleotide as the starting point.

In the human genome 13 distinct vertebrate specific RNase genes have been identified, all localized in chromosome 14 [1]. The pancreatic ribonuclease A (RNase A) superfamily, the only enzyme family restricted to vertebrates [2], comprises pyrimidine specific secreted endonucleases that degrade RNA through a two-step transphosphorolytic-hydrolytic reaction [3]. Several members of this superfamily are involved in angiogenesis and in the immune response system, displaying pathological side-effects during cancer and inflammatory disorders [4–7]. These unusual biological activities are critically dependent on their ribonucleolytic activity, a fact that portrays these RNases as attractive targets for the development of potent inhibitors for therapeutic intervention. Hence, structure assisted inhibitor design efforts have targeted human ribonucleases, angiogenin (RNase 5; Ang), eosinophil derived neurotoxin (RNase 2; EDN), and eosinophil cationic protein (RNase 3; ECP) [8].

The RNases active site consists of several subsites that accommodate the various phosphate, base, and ribose moieties of the substrate RNA. These subsites are designated as $P_o \ldots P_n$, $B_o \ldots B_n$, and $R_o \ldots R_n$, respectively [9]. The phosphate group where phosphodiester bond cleavage occurs binds in subsite P_1 (Gln11, His12, Lys41, His119). The nucleotide bases on the 3′ and 5′ sides of the scissile bond bind in B_1 (Thr45, Asp83, Phe120, and Ser123), and B_2 (Asn67,

Abbreviations
IMP, pdUppA-3′-p, 5′-phospho-2′-deoxyuridine 3-pyrophosphate (P′ → 5′) adenosine 3′-phosphate; RNase A, bovine pancreatic ribonuclease A.

Gln69, Asn71, Glu111 and His119), respectively. In addition, the 5′-phosphate group of a nucleotide bound at B_1 interacts with P_0 (Lys66) [9,10]. The existence of another subsite P_{-1} (Arg85) that interacts with the phosphate of a nucleotide bound in B_0 [11] has been confirmed by mutagenesis experiments [12]. The three catalytic residues His12, Lys41, and His119 of the P_1 subsite are present in all RNase homologs. The key B_1 residue, Thr45, is also maintained, but the other components of this subsite are variable. The B_2 subsite is fully or partially conserved while subsites P_{-1} and P_0 are least conserved among RNase homologs. Despite cross-homolog differences in B_1 and B_2 site structures, all members of the RNase family prefer pyrimidines at B_1 and purines at B_2. The high degree of conservation in the central region of the active site ($B_1P_1B_2$) has driven structure assisted inhibitor design studies to focus mainly on the parental protein, RNase A, as inhibitors developed against this enzyme could also inhibit other members of the superfamily. Today several inhibitors, mainly substrate analogs, mono and diphosphate (di)nucleotides with adenine at the 3′ position, and cytosine or uracyl at the 5′position of the scissile bond have been studied [13,14]. Purines bind at the B_2 subsite of RNase A which has been shown to exhibit a strong base preference in the order A > G > C > U [15]. However, only the interactions of adenine in the B_2 site have been examined by crystallography or NMR (complexes with $d(Ap)_4$ [16], d(CpA) [17,18], UpcA [19,20], 2′,5′, CpA [18,21], d(ApTpApA) [11], ppA-3′-p, ppA-2′-p [22], 3′,5′-ADP, 2′,5′-ADP, 5′ADP [14], dUppA-3′-p [23], pdUppA-3′-p [13]), thus far. All these compounds are rather marginal inhibitors with dissociation constants in the mid-to-upper μM range (the best inhibitor so far is pdUppA-3′p with K_i values of 27 nM, 180 nM and 260 nM for RNase A, EDN and RNase-4, respectively [13,24]) whereas transition state theory predicts pM values for genuine transition state analogs.

In all the RNase A–inhibitor complexes studied so far an adenine was bound in the B_2 subsite. In the quest for potent ribonucleolytic inhibitors we wanted to explore the potential of inosine as an alternative nucleotide to adenosine. Kinetics showed that IMP is a moderate inhibitor of the enzyme. In this report we present a high resolution (1.5 Å) crystal structure of the RNase A–IMP complex (Table 1), which reveals the molecular interactions at the active site and suggests ways to develop RNase A inhibitors that might bind more tightly. The crystal structure of the RNase A–AMP complex, at 1.5 Å resolution, was also determined for comparative reasons. The crystal structure of the RNase A–IMP complex indicated that three IMP molecules bind at the catalytic cleft in a novel binding mode by occupying the $B_1P_1B_2P_0P_{-1}$ region. In contrast, one AMP molecule binds at the active site of RNase A, occupying the P_1B_2 region. The crystal structure of the RNase A–IMP complex elucidates the structural determinants of the unusual binding mode of IMP to RNase A, and it also provides structural evidence for the key element of the P_{-1} subsite.

Table 1. Crystallographic statistics.

Protein complex	RNase A–IMP	RNase A–AMP
Resolution (Å)	20–1.54	30–1.50
Reflections measured	678501	228424
Unique reflections	32622	35273
R_{symm} [a]	0.041 (0.199)	0.041 (0.340)
Completeness (%)	97.4 (86.0)	98.1 (99.7)
$< I/\sigma I >$	18.7 (7.6)	10.4 (2.8)
R_{cryst} [b]	0.187 (0.205)	0.193 (0.240)
R_{free} [c]	0.234 (0.263)	0.231 (0.249)
No of solvent molecules	360	330
R.m.s. deviation from ideality		
in bond lengths (Å)	0.010	0.011
in angles (°)	1.42	1.46
Average B factor		
Protein atoms (Å^2) (mol A/mol B)	20.4/19.0	26.2/26.2
Solvent molecules (Å^2)	32.8	33.4
Ligand atoms (Å^2)[d]	37.5/29.8/21.8	23.4/38.8

[a] $R_{symm} = \Sigma_h\Sigma_i|I(h)-I_i(h)/\Sigma_h\Sigma_i I_i(h)$ where $I_i(h)$ and $I(h)$ are the ith and the mean measurements of the intensity of reflection h. [b] $R_{cryst} = \Sigma_h|F_o-F_c|/\Sigma_h F_o$, where F_o and F_c are the observed and calculated structure factors amplitudes of reflection h, respectively. [c] R_{free} is equal to R_{cryst} for a randomly selected 5% subset of reflections not used in the refinement [62]. [d] Values refer to IMP molecules I, II, and III in RNase A molecule A of the noncrystallographic dimer and AMP molecules I and II in RNase A molecules A and B, respectively, of the noncrystallographic dimer. Values in parentheses are for the outermost shell (RNase A–IMP: 1.58–1.54 Å; RNase A–AMP: 1.53–1.50 Å).

Results

Overall structures

Two RNase A molecules (A and B) exist in the crystallographic asymmetric unit [22]. Three IMP molecules are bound at the active site of mol A of the noncrystallographic RNase A dimer but two at the active site of mol B. The inhibitor molecules are well defined within the electron density map, only in the active site of mol A. In the active site of mol B, the electron density is poor hence our analysis has been focused only in the inhibitor complex in mol A. This partial binding, which has also been observed in previous binding studies with monoclinic crystals of RNase A [14,22],

has been attributed to the lattice contacts that limit access to the active site of mol B in the asymmetric unit.

In all free RNase A structures reported so far the side chain of the catalytic residue His119 adopts two conformations denoted as A ($\chi 1 = \approx 160°$) and B ($\chi 1 = \approx -80°$), which are related by a 100° rotation about the Cα–Cβ bond and a 180° rotation about the Cβ–Cγ bond [25–28]. These conformations are dependent on the pH [29], and the ionic strength of the crystallization solution [30]. In both the IMP and the AMP complexes, the side chain of His119 adopts conformation A (IMP: $\chi 1 = 148°$, AMP: $\chi 1 = 157°$) in agreement with previous studies that have shown that binding of sulphate or phosphate groups in P_1 induces conformation A [31].

Upon binding to RNase A, the three IMP molecules displace 10 water molecules from the active site of the free enzyme. With the exception of a shift of the side chain of Gln69 (constituent of the B_2 subsite) and a movement by ≈3.0 Å of the Arg85 (the sole component of the P_{-1} subsite [12]) side chain from its position in the free enzyme towards the inhibitor, there are no other significant conformational changes in the catalytic site of RNase A upon IMP binding. The r.m.s.d. between the structures of free RNase A (pdb code 1afu [22]), and the RNase A–IMP complex are 0.56, 0.52 and 0.88 Å for Cα, main chain and side chain atoms of 124 equivalent residues, respectively.

On binding, AMP displaces 4 water molecules from the active site of the free enzyme. There are no significant conformational changes due to AMP binding at the active site of RNase A. The r.m.s.d. between the RNase–AMP complex and the unliganded protein are 0.43, 0.44 and 0.59 Å for the Cα, main chain and side chain atoms of 123 equivalent residues, respectively. The r.m.s.d. between the IMP and the AMP complexes are 0.28, 0.32 and 0.90 Å for Cα, main chain and side chain atoms of 122 structural equivalents, respectively.

The binding of IMP to RNase A

The kinetic results showed that IMP is a moderate competitive inhibitor of the enzyme with a $K_i = 4.6 \pm 0.2$ mM in pH 5.5 (the pH of the crystallization medium). An electron density map calculated from X-ray data from RNase A crystals, soaked with 15 mM of IMP (the highest concentration used for the kinetic experiments) in the crystallization media for 2 h, showed only IMP mol I bound in the active site of the enzyme. It seems that this ligand molecule has the highest affinity in comparison to the other two IMP molecules and therefore the inhibition profile of IMP observed in the kinetic experiments corresponds only to the binding of IMP mol I to RNase A.

All atoms of the three IMP molecules (I, II, and III) are well defined within the sigmaA weighted Fo-Fc and 2Fo-Fc electron density maps of the RNase A–IMP complex (Fig. 1). Although the structure presented here is based on soaking experiment, data from RNase A cocrystallized with 100 mM were also available at 2.0 Å resolution. Preliminary analysis of this structure showed that the inhibitor is bound in exactly the same way as in the soaked crystal.

Upon binding to RNase A each of the three IMP molecules adopts a different conformation. The glycosyl torsion angle χ of IMP molecules I and II, adopts the frequently observed *anti* conformation [32], whereas in molecule III adopts the unusual *syn* conformation (Table 2). The ribose adopts the quite rare C4′-exo puckering in IMP molecules I and II. In contrast, the ribose adopts the C3′-endo conformation in molecule III, which is one of the preferred orientations for bound and unbound nucleotides [32]. The rest of the backbone and phosphate torsion angles are in the preferred range for protein bound purines [32] with the exception of the torsion angle ε which is in the unusual

Fig. 1. A schematic diagram of the RNase A molecule with the three IMP molecules bound at the active site. The sigmaA 2|Fo|–|Fc| electron density map calculated from the RNase A model before incorporating the coordinates of IMP, is contoured at 1.0 σ level, and the refined structure of the inhibitor is shown in red, green and cyan for IMP molecules I, II, and III, respectively.

Table 2. Torsion angles for IMP and AMP when bound to RNase A. Definitions of the torsion angles are according to the current IUPAC-IUB nomenclature [63], and the phase angle of the ribose ring is calculated as described previously [64]. For atom definitions see Scheme 1.

Protein	IMP I	IMP II	IMP III	AMP
Backbone torsion angles				
O5′-C5′-C4′-C3′ (γ)	−66 (*–sc*)	−160 (*ap*)	−171 (*ap*)	26 (sp.)
C5′-C4′-C3′-O3′ (δ)	125 (*+ac*)	87 (*+sc*)	105 (*+ac*)	126 (*+ac*)
C5′-C4′-C3′-C2′	−118	−157	−136	−113
C4′-C3′-C2′-O2′	−101	−92	−105	−143
Glycosyl torsion angle				
O4′-C1′-N9-C4 (χ)	−76 (*anti*)	−99 (*anti*)	75 (*syn*)	−44 (*anti*)
Pseudorotation angles				
C4′-O4′-C1′-C2′ (v_0)	29	−19	2	−30
O4′-C1′-C2′-C3′ (v_1)	−25	−4	−11	32
C1′-C2′-C3′-C4′ (v_2)	13	23	16	−23
C2′-C3′-C4′-O4′ (v_3)	4	−35	−15	6
C3′-C4′-O4′-C1′ (v_4)	−21	35	8	15
Phase	63 (*C4′-exo*)	50 (*C4′-exo*)	11 (*C3′-endo*)	135 (*C1′-exo*)
Phosphate torsion angle				
P-O5′-C5′-C4′ (β)	153 (*ap*)	98 (*+ac*)	133 (*+ac*)	−152 (*ap*)
C4′-C3′-O3′-P (ε)	−72 (*–sc*)	−19 (sp.)	−30 (*–sc*)	−89 (*–sc*)

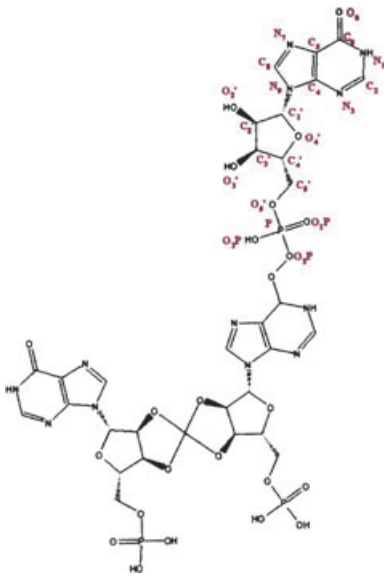

Scheme 1. The chemical structure of a putative ligand based on the binding mode of IMP to RNase A. The numbering scheme used for the IMP molecule is also shown in red.

–sc (IMP molecules I and III) or *sp* (IMP molecule II) range (Table 2). The numbering scheme used for IMP is shown in Scheme 1.

IMP molecule I binds to the active site by anchoring its phosphate group to subsite P_1 where it is involved in hydrogen bond interactions with the side chains of His12, Lys41, His119 (the catalytic triad), Gln11 and the main chain oxygen of Phe120 (Fig. 2A, Table 3). The ribose binds at R_2 toward subsite P_2 where atom O4′ is involved in a hydrogen bond interaction with Nε of Lys7. The purine base is located at the boundaries of the B_2 subsite with atom N1 in hydrogen-bonding distance from the side chain of Glu111 (Fig. 2A).

IMP mol II is bound at the active site with its inosine base just after the phosphate group of IMP mol I. In fact, N1 of IMP mol II and O2P from mol I are in hydrogen bonding distance (2.6 Å). The nucleotide base of IMP mol II, binds at subsite B_1 where atoms O6 and N7 form hydrogen bonds with Thr45. The ribose is situated in subsite P_0 and the hydroxyl O2′ group makes a hydrogen bond with the size chain of Lys66 (Fig. 2B, Table 3). The phosphate group of IMP mol II binds at the P_{-1} subsite within a hydrogen-bonding distance from the side chain of Arg85, which moves 5.0 Å (Cζ–Cζ distance) away from its position in the free enzyme toward the ligand. It is the first time that a hydrogen bond interaction between the side chain of Arg85 and a phosphate group of a ligand, has been observed. This provides further evidence for the involvement of Arg85 in the P_{-1} subsite, which has been inferred only by mutagenesis experiments [12].

The third IMP molecule (III) binds at the active site of RNase A with its nucleobase close to the C-terminus of the protein, the ribose at P_0, forming a hydrogen bond with the side chain of Lys66, and the phosphate group away from the protein towards the solution. IMP molecules III and II participate in a hydrogen bond network with their hydroxyl O2′

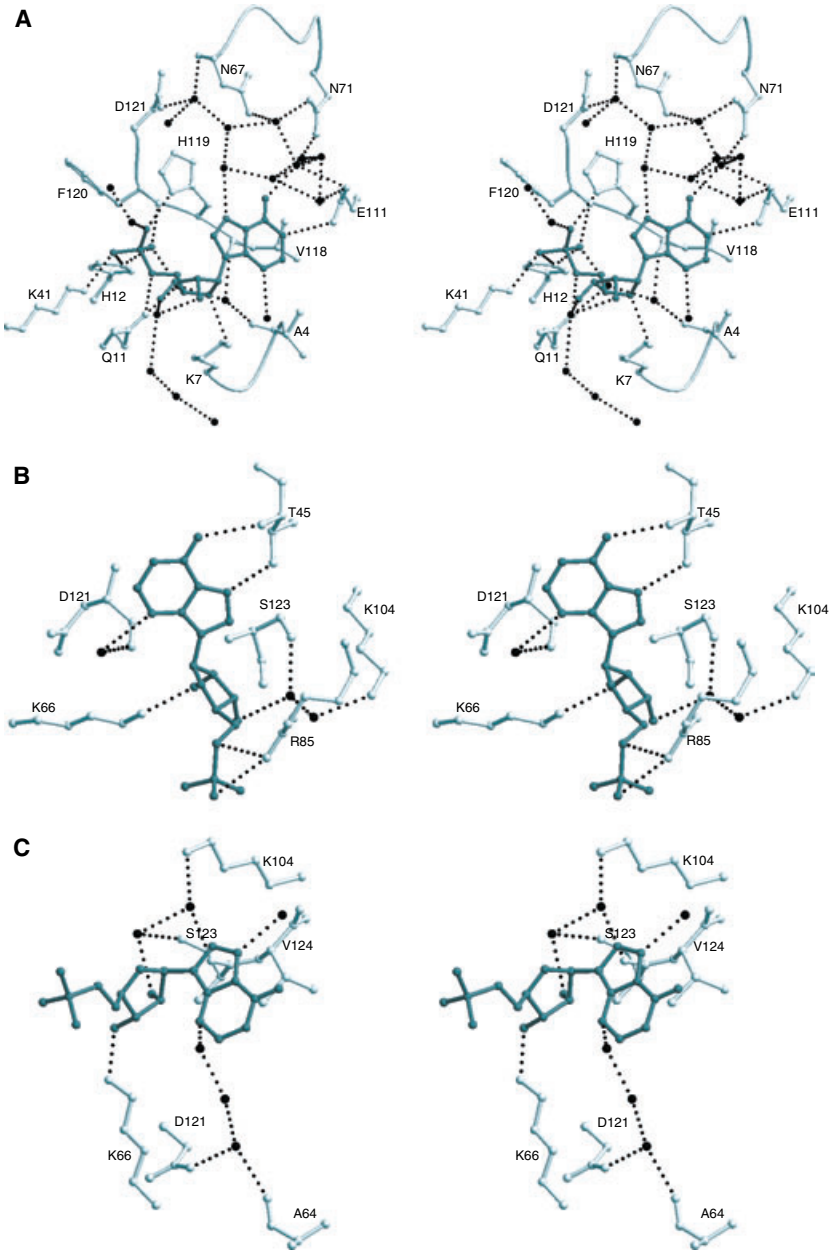

Fig. 2. Stereodiagrams of the interactions between RNase A and IMP molecules I (A), II (B), and III (C) in the active site. The side chains of protein residues involved in ligand binding are shown as ball-and-stick models. Bound water molecules are shown as black spheres. Hydrogen bond interactions are represented in dashed lines.

and O3′ groups (Fig. 2C, Table 3). In addition, the phosphate group of mol I is involved in 2 van der Waals interactions with the inosine base of mol II, while the ribose of mol II is involved in 9 non–polar interactions with atoms from the ribose of IMP mol III. Moreover, the three IMP molecules and RNase A participate in a complex water mediated hydrogen bonding network that involves 28 water molecules and 15 RNase A residues. On binding at the active site the three IMP molecules participate in a nonpolar network of 55 van der Waals interactions that includes also 17 protein residues (Table 4).

Upon binding to RNase A, IMP molecules I and II become more buried than mol III. Thus, the solvent accessibilities of the free ligand molecules are 468, 489 and 483 $Å^2$ for IMP molecules I, II, and III, respectively. When bound their accessible molecular surfaces shrink to 190 and 192 $Å^2$ in IMP molecules I and II, whereas in mol III becomes 357 $Å^2$. This indicates that 60% of the IMP surface in mol I and II becomes buried but only 26% in mol III. The greatest contribution for IMP mol I comes from the polar groups that contribute 189 $Å^2$ (68%) of the surface, which becomes inaccessible. For IMP molecules II and III,

Table 3. Potential hydrogen bonds of IMP and AMP with RNase A in the crystal. Hydrogen bond interactions were calculated with the program HBPLUS [65].Values in parentheses are distances in Å.

	RNase A–IMP			RNase A–AMP	
IMP/AMP atom	IMP Mol I	IMP Mol II	IMP Mol III	RNase A Mol A	RNase A Mol B
O6/N6	Water (2.6)	Thr45 N (2.9)		Asn71 Oδ1 (2.8)	Asn71 Oδ1 (3.0)
N6				Cys65 Sγ (3.3)	Cys65 Sγ (2.7)
N1	Glu111 Oε1 (3.0)			Asn71 Nδ2 (3.2)	Gln69 Oε1 (2.9)
N3	Water (2.8)	Water (3.3)	Water (2.2)	Water (2.8)	
N7	Water (2.9)	Thr45 Oγ1 (2.7)	Water (2.6)	Water (2.9)	Water (2.9)
O2′	Water (2.9)	Lys66 Nζ (2.7)	Water (2.9)	Water (2.8)	
O3′	Water (2.5)	Water (3.1)	Lys66 Nζ (2.5)		
O4′				Water (2.6)	
O5′	Gln11 Nε2 (2.8)	Arg85 Nη1 (3.0)		His119 Nδ1 (2.7)	
O1P	His12 Nε2 (2.7)			His12 Nε2 (2.7)	His12 Nε2 (3.0)
O1P	Phe120 N (2.9)			Phe120 N (3.0)	Phe120 N (2.9)
O1P	Water (2.9)			Water (2.8)	Water (2.8)
O2P	Lys41 Nε (2.7)			Gln11 Nε2 (2.6)	Gln11 Nε2 (3.0)
O3P	His119 Nδ1 (2.6)	Arg85 Nη1 (3.0)		Water (2.2)	Water (3.0)
O3P	Water (2.6)				

there is an equal contribution of the polar and nonpolar groups to the buried surface. On the protein surface, a total of 476 Å^2 solvent accessible surface area becomes inaccessible on binding of the three IMP molecules. The total buried surface area (protein plus 3 ligands) for the RNase A–IMP complex is 1065 Å^2. The shape correlation statistic Sc, which is used to quantify the shape complementarity of interfaces and gives an idea of the 'goodness of fit' between two surfaces [33] is 0.73, 0.72, and 0.69 for the association of the three IMP molecules to the active site, and 0.79 for the combined molecular surface of the three IMP molecules.

The binding of AMP to RNase A

In comparison to IMP, AMP is a more potent inhibitor of RNase A. Thus, K_i values of 46 μM [34] and 80 μM ([35], have been reported using CpG and C>p as substrates, respectively, at pH 5.9. RNase A crystals were soaked with a 200 mM AMP solution, 2.5-fold the concentration of IMP in the respective soaking experiment but in contrast to IMP there is only one molecule of AMP bound at the active site. All atoms of the AMP molecule are well defined within the sigmaA weighted F_o-F_c and $2F_o$-F_c electron density maps of the RNase A–AMP complex in both protein molecules in the asymmetric unit. However, in RNase mol A, there was additional density for an alternative conformation of the ribose and the phosphate (Fig. 3). Including this alternative AMP conformation with occupancy value of 0.3, estimated by the electron density map peaks, in the refinement process resulted in a lower R_{free} value. The second AMP conformation has the phosphoryl group away from the P_1 subsite and as it is a minor conformation it was not included in the structural comparisons.

The conformation of AMP when bound to RNase A is similar to that observed previously for adenosine nucleotides bound at B_2 in the RNase A complexes with $d(pA)_4$ [16], d(ApTpApApG) [11], d(CpA) [17], and 3′,5′ADP [14], as well as to those frequently observed in the unbound and protein bound adenosines [32]. The glycosyl torsion angle χ adopts the *anti*-conformation and the rest of the backbone and phosphate torsion angles are in the preferred range for protein bound adenosines [32]. The γ torsion angle is in the unusual *sp* range but its value (26°) is close to the favorable *+sc* range (30°–90°) (Table 2). The ribose is found at the *C1′-exo* conformation.

The binding of AMP is similar in both RNase A molecules of the noncrystallographic dimer. The inhibitor binds to the P_1B_2 region of the catalytic site with the 5′-phosphate group in P_1 involved in hydrogen bond interactions with Gln11, His12, and Phe120 (Table 3, Fig. 4). AMP binding mode is similar to that of 3′,5′ADP [14] with the adenine at B_2, involved in hydrogen bond interactions with the side chain of Asn71, and π–π interactions of the five-membered ring to the imidazole of His119 (Fig. 4). AMP forms hydrogen bonds with 6 and 3 water molecules in RNase molecules A and B, respectively, which mediate polar interactions with RNase A residues (Fig. 4). AMP atoms and 9 RNase A residues are involved in 40 and

Table 4. Van der Waals interactions of IMP and AMP in the active site of RNase A.

IMP/AMP atom	RNase A–IMP			RNase A–AMP	
	IMP Mol I	IMP Mol II	IMP Mol III	RNase A Mol A	RNase A Mol B
O6/N6 atom	His119, Cβ	His12, Cε1; Asn44, Cα, C	Val124, Cγ1	Cys65, Sγ; Gln69, Cβ, Cδ; Asn71, Cγ; Ala109, Cβ	Cys65, Cβ, Sγ; Gln69, Cβ, Cδ; Ala109, Cβ
C6	Val118, Cγ2; His119, Cβ	His12, Cε1, Asn44, Cα, Phe120, Cβ, Cδ1		Gln69, Cδ, Oε1; Ala109, Cβ	Gln69, Cδ, Oε1; Ala109, Cβ
C5	His119, Cβ	Asn44, Cα; Phe120, Cδ1	Val124, Cβ, Cγ1	His119, Cγ, Cδ2	Asn67, Nδ2; Ala109, Cβ; His119, Cγ
C4		Val43, Cγ1	Val124, Cγ1	His119, Cβ, Cγ, Cδ2	His119, Cβ, Cγ
C2	Val118, Cβ	Phe120, O		Ala109, Cβ; Glu111, Cδ, Oε1; Val118, Cγ2	Ala109, Cβ; Glu111, Oε1; Val118, Cγ2
N1	Val118, Cβ, Cγ2			Asn71, Nδ2; Ala109, Cβ	Asn71, Nδ2; Ala109, Cβ
N7	His119, Cβ, Cγ	Thr45, Cβ	Val124, Cβ, Cγ1	Asn67, Cγ, Nδ2; His119, Cδ2	Asn67, Cγ, Nδ2; His119, Cε1
C8		Val43, Cγ2; Thr45, Oγ1	Thr3, Cγ2; Ser123, O; Val124, Cα, Cγ1	His119, Cγ, Nδ1, Cε1, Nε2, Cδ2	His119, Cγ, Nδ1, Cε1, Nε2, Cδ2
N9				His119, Cγ	His119, Cγ, Cδ2
C1′			Ser123, O	His119, Cγ, Nδ1	His119, Cγ
C2′			Ala122, Cβ; Ser123, O	His119, Nδ1, Cε1	His119, Cδ2
O2′		Ala122, Cα			
C3′			Lys66, Cε, Nζ		His119, Cδ2
O3′			Lys66, Cε		
C4′	Lys7, Cε				His119, Cδ2
O4′	Lys7, Cε	Val43, Cγ1		His119, Cβ	His119, Cβ, Cγ, Cδ2
C5′	Gln11, Nε2	Arg85, Cζ, Nη1, Nη2		His119, Cα, Cβ, Nδ1	His119, Cγ,Cδ2
O5′					His119, Cδ2
P	His12, Nε2	Arg85, Nη1		His12, Nε2; His119, Nδ1	His12, Nε2; His12, Nε2
O1P	His119, Cα, C			His12, Cδ2; His119, Cα	His12, Cδ2; His119, Cα, Cδ2
O2P	His12, Cε1, Lys41, Cε				
O3P					His119, Cδ2
Total	17 contacts (6 residues)	20 contacts (7 residues)	16 contacts (5 residues)	40 contacts (9 residues)	44 contacts (9 residues)

44 van der Waals contacts in molecules A and B, respectively (Table 4).

Upon binding to RNase A, 67% of the AMP surface (330 Å^2) becomes inaccessible to the solvent, while the total buried surface area (protein plus ligand) for the RNase A–AMP complex is 532 Å^2 and 540 Å^2 in mol A and mol B, respectively. The shape correlation statistic Sc [33] is 0.77 for the association of AMP to the active site of RNase A.

Comparative structural analysis

Although the three IMP molecules bind to the catalytic cleft of RNase A one after the other, they do not follow a conventional pattern, i.e. base-ribose-phosphate-ribose-… (RNA motif), or a base-ribose-phosphate-base-… motif. In contrast the nucleotide sequence pattern is base$_1$-ribose$_1$-phosphate$_1$-base$_2$-ribose$_2$-ribose$_3$-base$_3$ (subscripts denote ligand molecule) while the phosphate groups of IMP molecules II and III point away from the nucleotide backbone.

Superposition of the RNase A–IMP complex onto the d(pA)$_4$ [16], d(ApTpApApG) [11], or d(CpA) [17] RNase A complexes where the nucleotides bind at the $B_1R_1P_1$- $B_2R_2P_2$ region of the active site, shows that IMP molecules I and II are close to the positions of the nucleotides that bind to $B_1R_1P_1$ and $B_2R_2P_2$, respectively, while IMP mol III does not superimpose with any of the building blocks of these two polynucleotide substrate analogs. There are no significant differences in conformation of the residues in the active site except from those of Arg85 (mentioned above), Asn67, and Gln69 that adopt different conformations in every complex. Besides these similarities, the IMP binding mode differs significantly from the binding of these polynucleotide inhibitors. Thus, although the

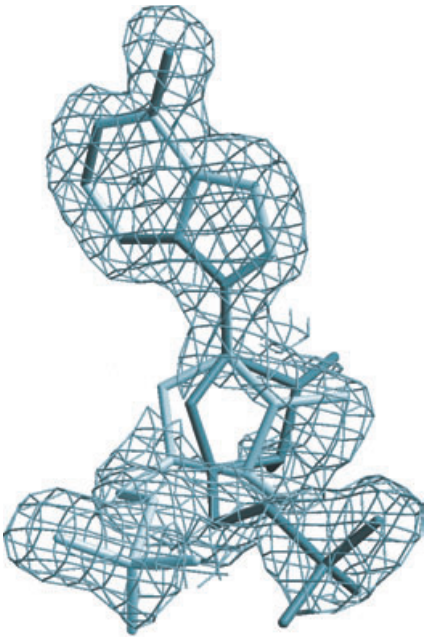

Fig. 3. The sigmaA 2|Fo|–|Fc| electron density map for the AMP bound in the active site of RNase A. The map was calculated from the RNase A model before incorporating the coordinates of AMP and is contoured at 1.0 σ level. The refined structure of the inhibitor is also shown as ball-and-stick model in white for the major conformation and grey for the minor.

nucleobase of IMP mol I is at the same plane with the purine ring of the nucleoside substrate that binds at B_2R_2, it is located 3.6 Å (O6-N6 distance) away from the purine's position at the B_2 subsite, superimposing onto the ribose in R_2 (Fig. 5B). However, the 5′-phosphate group of IMP mol I and the 5′-phosphoryl group of the substrate analogs, superimpose well at the P_1 subsite (phosphorus to phosphorous distance is ≈0.7 Å), while the ribose of IMP superimposes onto the 3′-phosphoryl group of the adenosine. The nucleobase of IMP mol II superimposes well with the substrate pyrimidine ring of the nucleotide that binds at B_2, and atoms O6 (IMP) and O2 (pyrimidine) are 0.6 Å apart (Fig. 5A). The rest of the IMP mol II is away from the nucleotide backbone as it is defined in the $d(Ap)_4$ complex [11] (Fig. 5A).

Superimposition of the RNase–IMP complex onto the RNase–AMP complex reveals that only the phosphoryl groups of IMP mol I and AMP superimpose well at the P_1 subsite (Fig. 5B). The rest of the inhibitor molecules do not superimpose with the nucleobase of IMP close to the position of the adenine of AMP in RNase A. The conformation of the active site RNase A residues is similar in the IMP and AMP complexes except Gln69 which in the IMP complex it adopts a conformation similar to that of the unliganded enzyme [22] pointing away from the B_2 subsite. Superposition of the RNase–IMP complex onto the RNase–pdUppA-3′-p complex [13] indicates a similar pattern with the difference that the phosphate group of IMP mol I is close to the position of the β-phosphate group of pdUppA-3′-p while the inosine base passes through the ribose of the adenosine part of pdUppA-3′-p (Fig. 5C).

Superposition of the RNase A–IMP complex onto the 3′,5′CpG [36], O^8-2′GMP [31], 2′,5′UpG [37], 2′CpG, dCpdG [38] complexes shows that IMP mol II superimposes onto the guanosine in subsite B_1 (Fig. 5D). The purine bases and the riboses superimpose well while the phosphate groups are 2.8 Å away. As a result the side chain of Arg85 adopts different conformations in the guanine and the IMP complexes that allow it to be in hydrogen-bonding distance to the phosphate group of guanosine or IMP.

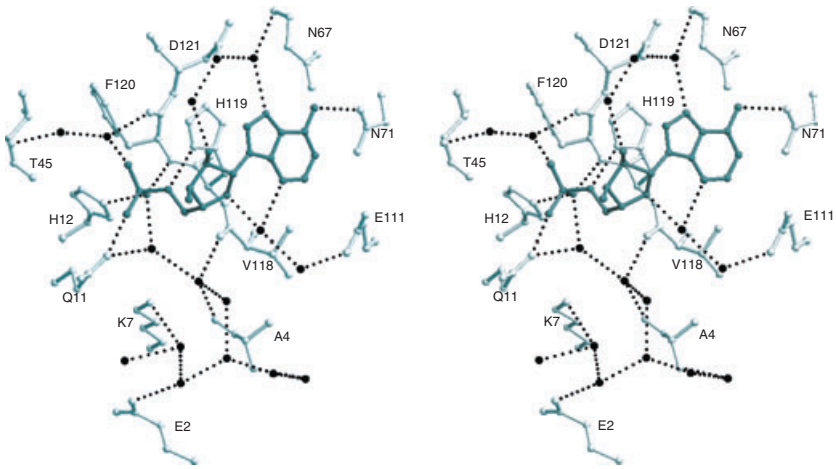

Fig. 4. Stereodiagrams of the interactions of AMP in the RNase A active site. The side chains of protein residues involved in ligand binding are shown as ball-and-stick models. Bound waters are shown as black spheres. Hydrogen bond interactions are represented in dashed lines.

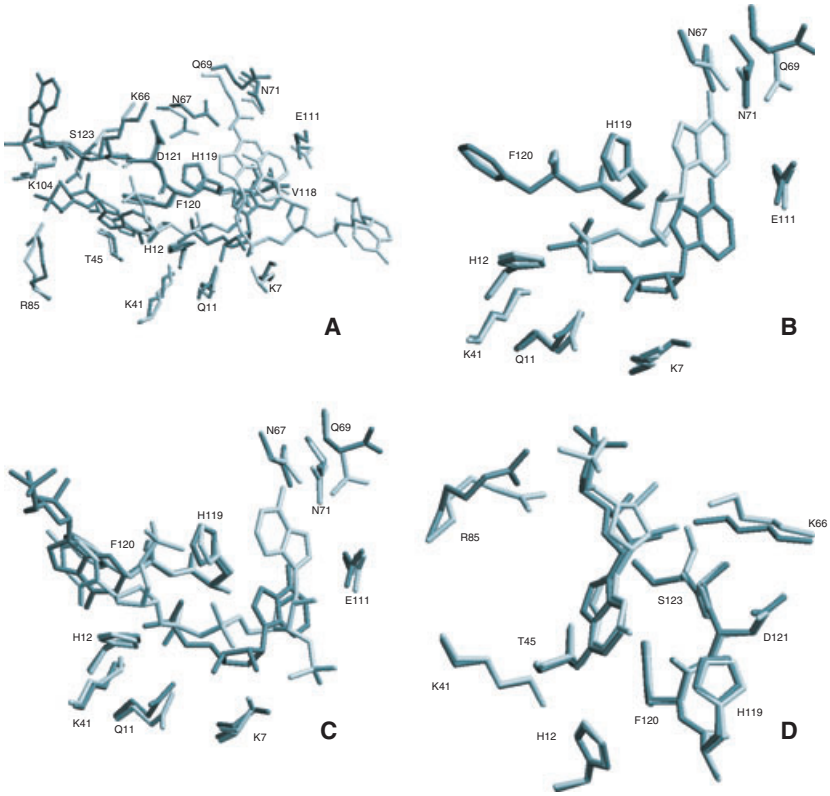

Fig. 5. Structural comparisons of the RNase A–IMP (grey) and RNase A–d(pA)$_4$ (A), RNase A–5′AMP (B), RNase A–pdUppA-3′p (C), and RNase A–d(CpG) (D) complexes (white).

Discussion

The binding of AMP supports the findings of previous structural studies with adenosine bound in subsite B_2. These indicated that Cys65, Asn67, Gln69, Asn71, Ala109, Glu111, and His119 are the residues that contact adenine. In most of the crystal structures [11,13,14,21,22] and in the RNase A mol B–AMP complex, both Gln69 and Asn71 hydrogen bond to the base while in the RNase A mol A–AMP complex and others [17,20], only Asn71 hydrogen bonds to adenine (Oδ1 to N6 and Nδ2 to N1). In virtually all of the RNase A-nucleotide complexes and in the AMP complex, the imidazole group of His119 is involved in stacking interactions with the five-membered ring of adenine. This is a highly favourable arrangement that contributes significantly to binding of purines. In addition, Cys65 Sγ and Ala109 Cβ are within van der Waals contact distance of the base. The functional role of Gln69, Asn71 and Glu111 has been analysed by kinetic and mutagenesis studies [39]. Substitution of Asn71 has a profound effect to the activity toward CpA (46-fold decrease), whereas substitutions of Gln69 and Glu111 do not affect the hydrolysis reaction with C>p as substrate [39]. This functional role of Asn71 is further supported by the present study since it seems that this residue is the key factor that impedes the binding of inosine to the B_2 subsite.

Crystallographic studies of RNase A in complex with guanine-containing mono- and dinucleotides (3′,5′CpG [36] O^8-2′GMP [31]; 2′,5′UpG [37]; 2′CpG, dCpdG [38]) showed that guanine does not bind in B_2 but in B_1, in a nonproductive binding mode designated as 'retro-binding' [40]. In a productive complex of a guanine-containing oligonucleotide (2′,5′UpG) to RNase A the uridine base is bound in B_1 while no electron density has been detected for the guanine base in the region of Glu111 [37]. The B_2 subsite does not bind the inosine base either closely. The main reason seems to be the carbonyl O6 group of the inosine base. A modelling study where the N6 group of AMP was replaced by a carbonyl group in the RNase A–AMP complex showed that binding of IMP in a similar manner to AMP would place the carbonyl O6 of IMP 3.1–3.5 Å away from Oδ1 of Asn67, Oε1 of Gln69, and Oδ1 of Asn71 in the B_2. At the pH of the crystallization (5.5) these groups are not protonated and therefore they cannot form hydrogen bond interactions with the carbonyl O6 group of the inosine base to favour binding in this subsite. Thus, the IMP base binds in the outskirts of the B_2 subsite towards Glu111 which is available for hydrogen–bonding interactions,

in a position which could be derived by sliding parallel the nucleobase from the position of adenine in the AMP complex by ≈4 Å. This proximity of the IMP base to the Glu111 side chain atoms is in agreement with previous kinetic data reporting that the hydrolysis of CpG is affected by mutating Glu111 [39]. All these findings indicate that the B_2 site is an essential adenine-preference site and Asn71 is the key structural determinant of this specificity. Thus, it seems that the phosphoryl group that binds at P_1 in a manner similar to other nucleotides is the anchoring point for the binding of IMP mol I. The rest of the inhibitor molecule binds outside of the B_2 cleft in a conformation that allows it to exploit interactions with the side chain of Glu111.

The 3D structures of RNase A nucleotide complexes reveal that B_1 is a pocket formed by His12, Val43, Asn44, Thr45, Phe120, and Ser123. The B_1 site of RNase A has a preference for pyrimidines with a small preference for cytosine over uracil [15]. Thr45 forms two hydrogen bonds with pyrimidines: its main-chain NH donates a hydrogen to O2 of either base, and its Oγ1 can donate to N3 of cytosine or accept from N3 of uracil. In crystal structures of RNase A complexes with uridine nucleotides, the Thr45 side chain also hydrogen bonds with the carboxylate of Asp83 [41]; this contact is not present in complexes with cytidine nucleotides [17,42], where the Oγ1 hydrogen is unavailable for donation to Asp83 and the two side chains are >4 Å farther apart. Mutational studies [43,44] suggested that the hydrogen bond between Thr45 Oγ1 and N3 of the pyrimidine ring is functionally important, and that its strength is modulated by the additional interaction of the threonine side chain with Oδ1 of Asp83.

The crystal structure of the RNase A–$d(Ap)_4$ complex [16] shows that adenine can also bind in this site but in an opposite way to pyrimidines. The main-chain NH of Thr45 forms a hydrogen bond with N7 and the side chain Oγ1 accepts a hydrogen from N6. In the crystal structure of the RNase A–$d(Ap)_4$ complex [16] both the Oγ1 of Thr45 and Oδ1 of Asp83 are in hydrogen bonding distance from the N6 group of the adenine while the distance between them is quite long for a hydrogen bond interaction. IMP also binds in subsite B_1 but in an opposite way to adenine [31,37,38] and similar to guanine and pyrimidines [31,36–38], with the main-chain NH and the side chain Oγ1 of Thr45 forming hydrogen bonds with O6 and N7, respectively. Thus, in contrast to the binding of IMP mol I, the anchoring point of IMP mol II seems to be the inosine ring, which is involved in polar interactions with Thr45, the primary functional component of this site. It appears that IMP mol II binds to RNase A in the retro-binding mode observed previously for guanines [40] but with a difference in the phosphate group mentioned above.

IMP mol III binds in a mode that has not been observed before in any RNase A complex. It is involved in polar contacts with the side chain of Lys66, the single component of P_0, and non-polar interactions with Val124. However, the side chain of Lys66 hydrogen-bonds to the ribose and not to the phosphate group as it is expected from previous studies [45]. The close interaction of the riboses of IMP mol II and III (Fig. 1) seems to be the driving force for the binding mode of IMP mol III and the protein provides further interactions to stabilize it. The close contacts of the three IMP molecules that drive them to form a pseudo trinucleotide together with the retro-binding mode of IMP mol II may provide an explanation why AMP does not bind in a similar way. AMP would have to bind in B_1 subsite like IMP mol II, if it was to form a tri-nucleotide complex similar to that of IMP. However, retro-binding mode has not been observed for adenosines in B_1 probably due to repulsion of the N6 group by the main chain NH of Thr45 (the primary functional component of this subsite). Therefore, it appears that the main reason for the IMP binding is the stereochemistry of the tri-nucleotide complex and the retro-binding mode in B_1 that allows it to form upon binding to RNase A.

The shape correlation statistics Sc, for $d(pA)_4$, d(ApTpApApG), d(CpA), and pdUppA-3′-p are 0.71, 0.72, 0.72, and 0.76, respectively. All these values are smaller or similar to the Sc for the combined molecular surface of the three IMP molecules (0.79) indicating that the fitness of the IMP molecular surface onto the active site surface of RNase A is similar (if not better), to that of other polynucleotides. This leads to the suggestion that a chemical entity composed of three IMP molecules suitably connected might be a better inhibitor than IMP. Thus, the 5′ phosphate group of the IMP molecule might connect to the carbonyl O6 group of another IMP molecule and then the hydroxyl groups 2′ and 3′ from the ribose of the second IMP molecule could covalently bond through a carbon atom to the 2′, and 3′ hydroxyl groups of the ribose of a third IMP molecule producing the chemical entity shown in Scheme 1. Modelling studies indicated that this molecule might be accommodated within the RNase A active site without any steric impediments indicating that it could be an RNase A inhibitor, and we are currently pursuing its synthesis and study. Moreover, a suitable addition to the carbonyl O6 group of the first IMP molecule might allow the

exploitation of interactions with the side chains of Asn67, Gln69, and Asn71 in the B_2 subsite, enhancing further the potency of the inhibitor.

Conclusions

The present study presents the first RNase A–trimolecular nucleotide complex model, and by illuminating the structural determinants of the IMP binding to RNase A shows that the inhibitor binds to the enzyme in a novel mode. The chemical characteristics of the IMP molecule seem to impose this binding mode of IMP. Subsite B_2 does not bind inosine but the nucleobase is accommodated in the outskirts of subsite B_2 exploiting interactions with Glu111. IMP also follows the retro-binding mode previously observed for guanosine-containing mono- and dinucleotides [40] and binds to B_1. The structural analysis of the IMP binding has also provided structural evidence that Arg85 is a component of the P_{-1} subsite.

Rational design for new inhibitors requires detailed knowledge of the enzyme–ligand interactions and the present structural study at high resolution has provided the guidelines for the design of a new series of inosine-based inhibitors.

Experimental procedures

Kinetic experiments

Bovine pancreatic RNase A (type XII-A), IMP, AMP and C>p were obtained from Sigma-Aldrich (Athens, Greece). Concentrations of RNase A samples and substrate concentrations (C>p) were determined spectrophotometrically using absorption coefficients $\varepsilon_{278} = 9800\ \text{M}^{-1}\cdot\text{cm}^{-1}$ [46], and $\varepsilon_{268} = 8400\ \text{M}^{-1}\cdot\text{cm}^{-1}$ [47], respectively. Enzymatic activity of RNase A was measured by a spectrophotometric method [48]. All assays were performed at 25 °C in 0.2 M AcONa/AcOH (pH 5.5) in duplicate with enzyme concentrations 0.2 μM. The activity was measured by following the initial reaction velocities using a difference molar absorbance coefficient $\varepsilon_{296} = 516.4\ \text{M}^{-1}\cdot\text{cm}^{-1}$ for the hydrolysis reaction of C>p [48]. K_i values were determined by the Dixon method [49] using nonlinear regression analysis with the program GRAFIT [50] and three different substrate concentrations (0.3, 0.5 and 1.0 mM) against three inhibitor concentrations (7, 10, and 15 mM for IMP, and 1, 2, and 5 mM for AMP).

Crystallization, data collection and structure refinement

Crystals of RNase A were grown at 16 °C using the hanging drop vapour diffusion technique as described previously [22]. Crystals of the inhibitor complexes were obtained by soaking the RNase A crystals in 20 mM sodium citrate, pH 5.5, 25% PEG 4000 containing either 82 mM IMP or 200 mM AMP for 11 h and 18.5 h, respectively, prior to data collection.

Diffraction data for the RNase A inhibitor complexes to 1.5 Å resolution were collected on station X11 (λ = 0.8115 Å) EMBL/DESY, Hamburg, using a MAR CCD detector at 100 K. Data were processed using the HKL package [51] and intensities were transformed to amplitudes by the program TRUNCATE [52]. Phases were obtained using the structure of free RNase A from monoclinic crystals (pdb code: 1afk [22]); as starting model. Alternate cycles of manual building with the program O [53], and refinement using the maximum likelihood target function as implemented in the program REFMAC [54] improved the model. Inhibitor molecules were included during the final stages of the refinement. Details of data processing and refinement statistics are provided in Table 1.

The program PROCHECK [55] was used to assess the quality of the final structure. Analysis of the Ramachandran (φ-ψ) plot showed that all residues lie in the allowed regions. Solvent accessible areas were calculated with the program NACCESS [56]. Atomic coordinates and the X-ray amplitudes of the RNase A–IMP, and RNase A–AMP, complexes have been deposited in Research Collaboratory for Structural Bioinformatics Protein Data Bank (http://www.rcsb.org) (accession numbers 1Z6D and 1Z6S, respectively). Figures were prepared with the programs MOLSCRIPT [57] or BOBSCRIPT [58] and rendered with RASTER3D [59].

Modelling

The binding of a molecule produced by covalently linking the three IMP molecules (Scheme 1) to RNase A was studied by modelling. A 3D model of this molecule was generated by the program CORINA (http://www.2.ccc.uni-erlangen.de/software/corina/free_struct.html) [60]. This 3D model was fitted manually into the active site of RNase A by superimposing it on the three IMP molecules in the protein complex and by adjusting its torsion angles to fit the conformation of the three ligands. The resulting complex was then subjected to conjugate gradient minimization with no experimental energy terms as implemented in the program CNS [61].

Acknowledgements

We would like to thank Dr I. D. Kostas for valuable discussions during the writing of this study. This work was supported by the Hellenic General Secretariat for Research and Technology (GSRT), through a Joint Research and Technology project between Greece and Slovenia (2002–05) (to D.D.L and J.K). The assistance

of the staff at EMBL, Hamburg and SRS, Daresbury is also acknowledged for providing excellent facilities for X-ray data collection. This work was supported by grants from European Community – Research Infrastructure Action under the FP6 'Structuring the European Research Area Programme' for work at the Synchrotron Radiation Source, CCLRC, Daresbury UK (contract number HPRI-CT-1999–00012), and EMBL Hamburg Outstation, Germany (contract number RII3/CT/2004/5060008) to D.D.L and N.G.O.

References

1 Cho S, Beintema JJ & Zhang J (2005) The ribonuclease A superfamily of mammals and birds: identifying new members and tracing evolutionary histories. *Genomics* **85**, 208–220.
2 International Human Genome Sequencing Consortium. (2004) Finishing the euchromatic sequence of the human genome. *Nature* **431**, 931–945.
3 Beintema JJ & Kleineidam RG (1998) The ribonuclease A superfamily: general discussion. *Cell Mol Life Sci* **54**, 825–832.
4 Rosenberg HF & Domachowske JB (2001) Eosinophils, eosinophil ribonucleases, and their role in host defense against respiratory virus pathogens. *J Leukoc Biol* **70**, 691–698.
5 Venge P, Bystrom J, Carlson M, Hakansson L, Karawacjzyk M, Peterson C, Seveus L & Trulson A (1999) Eosinophil cationic protein (ECP): molecular and biological properties and the use of ECP as a marker of eosinophil activation in disease. *Clin Exp Allergy* **29**, 1172–1186.
6 Boix E (2001) Eosinophil cationic protein. *Methods Enzymol* **341**, 287–305.
7 Riordan JF (2001) Angiogenin. *Methods Enzymol* **341**, 263–273.
8 Russo A, Acharya KR & Shapiro R (2001) Small molecule inhibitors of RNase A and related enzymes. *Methods Enymol* **341**, 629–648.
9 Raines RT (1998) Ribonuclease A. *Chem Rev* **98**, 1045–1065.
10 Nogues MV, Moussaoui M, Boix E, Vilanova M, Ribo M & Cuchillo CM (1998) The contribution of noncatalytic phosphate-binding subsites to the mechanism of bovine pancreatic ribonuclease A. *Cell Mol Life Sci* **54**, 766–774.
11 Fontecilla-Camps JC, de Llorens R, Du le, MH & Cuchillo CM (1994) Crystal structure of ribonuclease A·d(ApTpApApG) complex. *J Biol Chem* **269**, 21526–21531.
12 Fisher BM, Grilley JE & Raines RT (1998) A new remote subsite in ribonuclease A. *J Biol Chem* **273**, 34134–34138.
13 Leonidas DD, Shapiro R, Irons LI, Russo N & Acharya KR (1999) Toward rational design of ribonuclease inhibitors: high-resolution crystal structure of a ribonuclease A complex with a potent-3′,5′-pyrophosphate-linked dinucleotide inhibitor. *Biochemistry* **38**, 10287–10297.
14 Leonidas DD, Chavali GB, Oikonomakos NG, Chrysina ED, Kosmopoulou MN, Vlassi M, Frankling C & Acharya KR (2003) High-resolution crystal structures of ribonuclease A complexed with adenylic and uridylic nucleotide inhibitors. Implications for structure-based design of ribonucleolytic inhibitors. *Protein Sci* **12**, 2559–2574.
15 Witzel H & Barnard EA (1962) Mechanism and binding sites in the ribonuclease reaction II. Kinetic studies on the first step of the reaction. *Biochem Biophys Res Commun* **7**, 295–299.
16 McPherson A, Brayer GD & Morrison RD (1986) Crystal structure of RNase A complexed with $d(pA)_4$. *J Mol Biol* **189**, 305–327.
17 Zegers I, Maes D, Dao-Thi M-H, Poortmans F, Palmer R & Wyns L (1994) The structures of RNase A complexed with 3′CMP and d(CpA): Active site conformation and conserved water molecules. *Protein Sci* **31**, 2322–2339.
18 Toiron C, Gonzalez C, Bruix M & Rico M (1996) Three-dimensional structure of the complexes of ribonuclease A with 2′,5′-CpA and 3′,5′-d(CpA) in aqueous solution, as obtained by NMR and restrained molecular dynamics. *Protein Sci* **5**, 1633–1647.
19 Richards FM & Wyckoff HW (1973) Ribonuclease S. *Atlas of Molecular Structures in Biology* Vol. 1 (Philips, D C & Richards, F M, eds). Clarendon, Oxford, UK.
20 Gilliland GL, Dill J, Pechik I, Svensson LA & Sjolin L (1994) The active site of bovine pancreatic ribonuclease: an example of solvent modulated specificity. *Protein Pept Lett* **1**, 60–65.
21 Wodak SY, Liu MY & Wyckoff HW (1977) The structure of cytidilyl (2′,5′) adenosine when bound to pancreatic ribonuclease S. *J Mol Biol* **116**, 855–875.
22 Leonidas DD, Shapiro R, Irons LI, Russo N & Acharya KR (1997) Crystal structures of ribonuclease A complexes with 5′-diphosphoadenosine 3′-phosphate and 5′-diphosphoadenosine 2′-phosphate at 1.7 Å resolution. *Biochemistry* **36**, 5578–5588.
23 Jardine AM, Leonidas DD, Jenkins JL, Park C, Raines RT, Acharya KR & Shapiro R (2001) Cleavage of 3,′5-pyrophosphate-linked dinucleotides by ribonuclease A and Angiogenin. *Biochemistry* **40**, 10262–10272.
24 Russo N & Shapiro R (1999) Potent inhibition of mammalian ribonucleases by 3′,5′-pyrophosphate-linked ucleotides. *J Biol Chem* **274**, 14902–14908.
25 Borkakoti N, Moss DA & Palmer RA (1982) Ribonuclease A: Least squares refinement of structure at 1.45 Å resolution. *Acta Crystallogr B* **38**, 2210–2217.

26 Howlin B, Moss DS & Harris GW (1989) Segmented anisotropic refinement of bovine ribonuclease A by the application of rigid-body tls model. *Acta Crystallogr A* **45**, 851–861.
27 deMel VSJ, Doscher MS, Martin PD & Edwards BFP (1994) The occupancy of two distinct conformations by active-site histidine-119 in crystals of Ribonuclease is modulated by pH. *FEBS Lett* **349**, 155–160.
28 Mazzarella L, Capasso S, Demasi D, Di'Lorenzo G, Mattia CA & Zagari A (1993) Bovine seminal ribonuclease – structure at 1.9 Å resolution. *Acta Crystallogr D* **49**, 389–402.
29 Berisio R, Lamzin VS, Sica F, Wilson KS, Zagari A & Mazzarella L (1999) Protein titration in the crystal state. *J Mol Biol* **292**, 845–854.
30 Fedorov AA, Joseph-McCarthy D, Fedorov E, Sirakova D, Graf I & Almo SC (1996) Ionic interactions in crystalline bovine pancreatic ribonuclease A. *Biochemistry* **35**, 15962–15979.
31 Borkakoti N (1983) The active site of ribonuclease A from the crystallographic studies of ribonuclease-A-inhibitor complexes. *Eur J Biochem* **132**, 89–94.
32 Moodie SL & Thornton JM (1993) A study into the effects of protein binding on nucleotide conformation. *Nucleic Acid Res* **21**, 1369–1380.
33 Lawrence MC & Colman PM (1993) Shape complementarity at protein/protein interfaces. *J Mol Biol* **234**, 946–950.
34 Irie M, Watanabe H, Ohgi K, Tobe M, Matsumura G, Arata Y, Hirose T & Inayama S (1984) Some evidence suggesting the existence of P2 and B3 sites in the active site of bovine pancreatic ribonuclease A. *J Biochem* **95**, 751–759.
35 Russo N, Shapiro R & Vallee BL (1997) 5′-diphosphoadenosine 3′-phosphate is a potent inhibitor of bovine pancreatic ribonuclease A. *Biochem Biophys Res Commun* **231**, 671–674.
36 Lisgarten JN, Maes D, Wyns L, Aguilar CF & Palmer RA (1995) Structure of the crystalline complex of deoxycytidylyl-3′,5′-Guanosine(3′,5′-Dcpdg) cocrystallized with ribonuclease at 1.9-angstrom resolution. *Acta Crystallogr D* **51**, 767–771.
37 Vitagliano L, Merlino A, Zagari A & Mazzarella L (2000) Productive and nonproductive binding to ribonuclease A: X-ray structure of two complexes with uridylyl(2′,5′)guanosine. *Protein Sci* **9**, 1217–1225.
38 Aguilar CF, Thomas PJ, Moss DS, Mills A & Palmer RA (1991) Novel non-productively bound ribonuclease inhibitor complexes – high resolution X-ray refinement studies on the binding of RNase-A to cytidylyl-2′,5′-guanosine (2′,5′CpG) and deoxycytidylyl-3′,5′-guanosine (3′,5′dCpdG). *Biochim Biophys Acta* **1118**, 6–20.
39 Tarragona-Fiol A, Eggelte HJ, Harbron S, Sanchez E, Taylorson CJ, Ward JM & Rabin BR (1993) Identification by site-directed mutagenesis of amino-acids in the B2 subsite of bovine pancreatic ribonuclease A. *Protein Eng* **6**, 901–906.
40 Aguilar CF, Thomas PJ, Mills A, Moss DS & Palmer RA (1992) Newly observed binding mode in pancreatic ribonuclease. *J Mol Biol* **224**, 265–267.
41 Wlodawer A, Miller M & Sjolin L (1983) Active site of RNase: neutron diffraction study of a complex with uridine vanadate, a transition state analog. *Proc Natl Acad Sci USA* **80**, 3628–3631.
42 Lisgarten JN, Gupta V, Maes D, Wyns L, Zegers I, Palmer RA, Dealwis CG, Aguilar CF & Hemmings AM (1993) Structure of the crystalline complex of cytidylic acid (2′-CMP) with ribonuclease at 1.6 Å resolution. Conservation of solvent sites in RNase-A high resolution structures. *Acta Crystallogr D* **49**, 541–547.
43 deI, Cardayre SB & Raines RT (1994) Structural determinants of enzymatic processivity. *Biochemistry* **33**, 6031–6037.
44 deI, Cardayre SB & Raines RT (1995) A residue to residue hydrogen bond mediates the nucleotide specificity of ribonuclease A. *J Mol Biol* **252**, 328–336.
45 Parés X, Nogués MV, Llorens R & Cuchillo CM (1991) Structure and function of ribonuclease A binding subsites. *Essays Biochem* **26**, 89–103.
46 Sela M & Anfinsen CB (1957) Some spectrophotometric and polarimetric experiments with ribonuclease. *Biochim Biophys Acta* **24**, 229–235.
47 Boix E, Nikolovski Z, Moiseyev GP, Rosenberg HF, Cuchillo CM & Nogués MV (1999) Kinetic and product distribution analysis of human eosinophil cationic protein indicates a subsite arrangement that favors exonuclease-type activity. *J Biol Chem* **274**, 15605–15614.
48 Boix E, Nogues MV, Schein CH, Benner SA & Cuchillo CM (1994) Reverse transphosphorylation by ribonuclease A needs an intact (P2) - binding site. Point mutations at Lys 7 and Arg 10 alter the catalytic properties of the enzyme. *J Biol Chem* **269**, 2529–2534.
49 Dixon M (1953) The determination of enzyme inhibitor constants. *Biochem J* **55**, 170–171.
50 Leatherbarrow RJ (1992) *Grafit, Version 3.0*. Erithacus Software Ltd, Staines, UK.
51 Otwinowski Z & Minor W (1997) Processing of X-ray diffraction data collected in oscillation mode. In *Methods Enzymol.* (Carter, C W J & Sweet, R M, eds), pp. 307–326. Academic Press, New York.
52 French S & Wilson KS (1978) On the treatment of the negative intensity observations. *Acta Crystallogr A* **34**, 517–525.
53 Jones TA, Zou JY, Cowan SW & Kjeldgaard M (1991) Improved methods for building models in electron density maps & the location of errors in these models. *Acta Crystallogr A* **47**, 110–119.
54 Murshudov GN, Vagin AA & Dodson EJ (1997) Refinement of macromolecular structures by the maximum-likelihood method. *Acta Crystallogr D* **53**, 240–255.

55 Laskowski RA, MacArthur MW, Moss DS & Thornton JM (1993) PROCHECK – A program to check the stereochemical quality of protein structures. *J Appl Crystallog* **26**, 283–291.
56 Hubbard SJ & Thornton JM (1993) *NACCESS*. Department of Biochemistry and Molecular Biology, University College, London, UK.
57 Kraulis PJ (1991) MOLSCRIPT – A program to produce both detailed & schematic plots of protein structures. *J Appl Crystallogr* **24**, 946–950.
58 Esnouf RM (1997) An extensively modified version of MOLSCRIPT that includes greatly enhanced coloring capabilities. *J Mol Graphics Modelling* **15**, 132–134.
59 Merritt EA & Bacon DJ (1997) RASTER3D: Photorealistic molecular graphics. *Methods Enzymol* **B277**, 505–524.
60 Sadowski J & Gasteiger J (1993) From atoms and bonds to 3-dimensional atomic coordinates – automatic model builders. *Chem Rev* **93**, 2567–2581.
61 Brunger AT, Adams PD, Clore GM, DeLano WL, Gros P, GrosseKunstleve RW, Jiang JS, Kuszewski J, Nilges M, Pannu NS, *et al*. (1998) Crystallography & NMR system: a new software suite for macromolecular structure determination. *Acta Crystallogr D* **54**, 905–921.
62 Brünger AT (1992) Free R value: a novel statistical quantity for assessing the accuracy of crystal structures. *Nature* **355**, 472–475.
63 IUPAC-IUB & (JCBN) JCoBN (1983) Symbols for specifying the conformation of polysaccharide chains. Recommendations 1981. *Eur J Biochem* **131**, 5–7.
64 Altona C & Sundaralingam M (1972) Conformational analysis of the sugar ring in nucleosides and nucleotides. A new description using the concept of pseudorotation. *J Am Chem Soc* **94**, 8205–8212.
65 McDonald IK & Thornton JM (1994) Satisfying hydrogen bonding potential in proteins. *J Mol Biol* **238**, 777–793.